Research Article
Experimental and Translational Hepatology

JOURNAL
OF HEPATOLOGY

Soluble TREM2 levels reflect the recruitment and expansion of TREM2$^+$ macrophages that localize to fibrotic areas and limit NASH

Graphical abstract

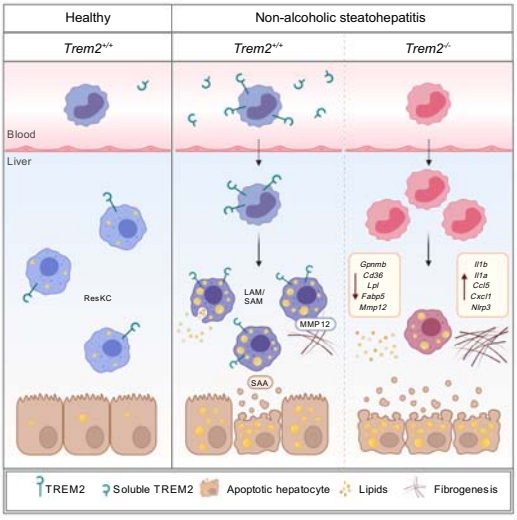

Highlights

- Systemic soluble TREM2 levels mirror NASH severity in mice and humans.
- TREM2$^+$ macrophages localize to areas of fibrosis.
- TREM2-deficient macrophages display decreased viability, profibrogenic potential and impaired lipid handling.
- Hematopoietic TREM2 protects from steatohepatitis and liver fibrosis.

Authors

Tim Hendrikx, Florentina Porsch, Máté G. Kiss, …, Matthias Farlik, Dennis Wolf, Christoph J. Binder

Correspondence

christoph.binder@meduniwien.ac.at (C.J. Binder), tim.hendrikx@meduniwien.ac.at (T. Hendrikx).

Lay summary

Our study defines the origin and function of macrophages (a type of immune cell) that are present in the liver and express a specific protein called TREM2. We find that these cells have an important role in protecting against non-alcoholic steatohepatitis (a progressive form of fatty liver disease). We also show that the levels of soluble TREM2 in the blood could serve as a circulating marker of non-alcoholic fatty liver disease.

https://doi.org/10.1016/j.jhep.2022.06.004
 J. Hepatol. 2022, 77, 1373–1385

Research Article
Experimental and Translational Hepatology

JOURNAL OF HEPATOLOGY

Soluble TREM2 levels reflect the recruitment and expansion of TREM2$^+$ macrophages that localize to fibrotic areas and limit NASH

Tim Hendrikx[1,2,*,†], Florentina Porsch[1,†], Máté G. Kiss[1], Dragana Rajcic[1], Nikolina Papac-Miličević[1], Constanze Hoebinger[1], Laura Goederle[1], Anastasiya Hladik[3], Lisa E. Shaw[4], Hauke Horstmann[9], Sylvia Knapp[3], Sophia Derdak[5], Martin Bilban[1,5], Lena Heintz[6], Marcin Krawczyk[6,7], Rafael Paternostro[8], Michael Trauner[8], Matthias Farlik[4], Dennis Wolf[9], Christoph J. Binder[1,*]

[1]*Department of Laboratory Medicine, KILM, Medical University Vienna, Vienna, Austria;* [2]*Department of Molecular Genetics, NUTRIM, Maastricht University, Maastricht, the Netherlands;* [3]*Department of Medicine I, Laboratory of Infection Biology, Medical University Vienna, Vienna, Austria;* [4]*Department of Dermatology, Medical University Vienna, Vienna, Austria;* [5]*Core Facilities, Medical University of Vienna, Medical University Vienna, Vienna, Austria;* [6]*Department of Medicine II, Saarland University Medical Center, Saarland University, Homburg, Germany;* [7]*Department of General, Transplant and Liver Surgery, Centre for Preclinical Research, Laboratory of Metabolic Liver Diseases, Medical University of Warsaw, Warsaw, Poland;* [8]*Department of Internal Medicine III, Division of Gastroenterology and Hepatology, Medical University Vienna, Vienna, Austria;* [9]*Department of Cardiology and Angiology I, Medical Center, University of Freiburg, Faculty of Medicine, Freiburg, Germany*

Background & Aims: Previous single-cell RNA-sequencing analyses have shown that *Trem2*-expressing macrophages are present in the liver during obesity, non-alcoholic steatohepatitis (NASH) and cirrhosis. Herein, we aimed to functionally characterize the role of bone marrow-derived TREM2-expressing macrophage populations in NASH.

Methods: We used bulk RNA sequencing to assess the hepatic molecular response to lipid-dependent dietary intervention in mice. Spatial mapping, bone marrow transplantation in two complementary murine models and single-cell sequencing were applied to functionally characterize the role of TREM2$^+$ macrophage populations in NASH.

Results: We found that the hepatic transcriptomic profile during steatohepatitis mirrors the dynamics of recruited bone marrow-derived monocytes that already acquire increased expression of *Trem2* in the circulation. Increased *Trem2* expression was reflected by elevated levels of systemic soluble TREM2 in mice and humans with NASH. In addition, soluble TREM2 levels were superior to traditionally used laboratory parameters for distinguishing between different fatty liver disease stages in two separate clinical cohorts. Spatial transcriptomics revealed that TREM2$^+$ macrophages localize to sites of hepatocellular damage, inflammation and fibrosis in the steatotic liver. Finally, using multiple murine models and *in vitro* experiments, we demonstrate that hematopoietic *Trem2* deficiency causes defective lipid handling and extracellular matrix remodeling, resulting in exacerbated steatohepatitis, cell death and fibrosis.

Conclusions: Our study highlights the functional properties of bone marrow-derived TREM2$^+$ macrophages and implies the clinical relevance of systemic soluble TREM2 levels in the context of NASH.

Lay summary: Our study defines the origin and function of macrophages (a type of immune cell) that are present in the liver and express a specific protein called TREM2. We find that these cells have an important role in protecting against non-alcoholic steatohepatitis (a progressive form of fatty liver disease). We also show that the levels of soluble TREM2 in the blood could serve as a circulating marker of non-alcoholic fatty liver disease.

Keywords: Metabolic-associated fatty liver disease; Steatohepatitis; TREM2+ macrophages; Soluble TREM2; Liver fibrosis; Spatial transcriptomics.
Received 17 August 2021; received in revised form 3 June 2022; accepted 7 June 2022; available online 21 June 2022
* Corresponding authors. Address: Department of Laboratory Medicine, KILM, Medical University Vienna, Vienna, Austria.
E-mail addresses: christoph.binder@meduniwien.ac.at (C.J. Binder), tim.hendrikx@meduniwien.ac.at (T. Hendrikx).
† Contributed equally as first authors.
https://doi.org/10.1016/j.jhep.2022.06.004

Introduction

Sedentary behavior and excess calorie intake have led to the high prevalence of lifestyle-related disorders, including non-alcoholic fatty liver disease (NAFLD), recently renamed as metabolic dysfunction-associated fatty liver disease (MAFLD).[1] NAFLD covers a spectrum of liver disease stages ranging from simple steatosis to more progressive inflammatory steatohepatitis (NASH), which increases the risk of developing fibrosis and cirrhosis, ultimately requiring a liver transplantation.[1,2] In fact, NASH is predicted to soon surpass viral hepatitis as the main cause of end-stage liver disease and become the primary indication for liver transplantation, thus posing a major clinical and economic burden.[3,4] Therefore, there is an unmet need to identify factors that can be targeted therapeutically to prevent NAFLD progression.

The presence of chronic low-grade inflammation characterized by immune cell activation, abnormal cytokine production and increased acute phase protein levels is a hallmark of NASH.[5,6] Particularly, macrophages are thought to represent key mediators responsible for the initiation and propagation of hepatic inflammation and the regulation of fibrosis.[7] Upon activation of resident Kupffer cells (ResKCs), proinflammatory cytokines and

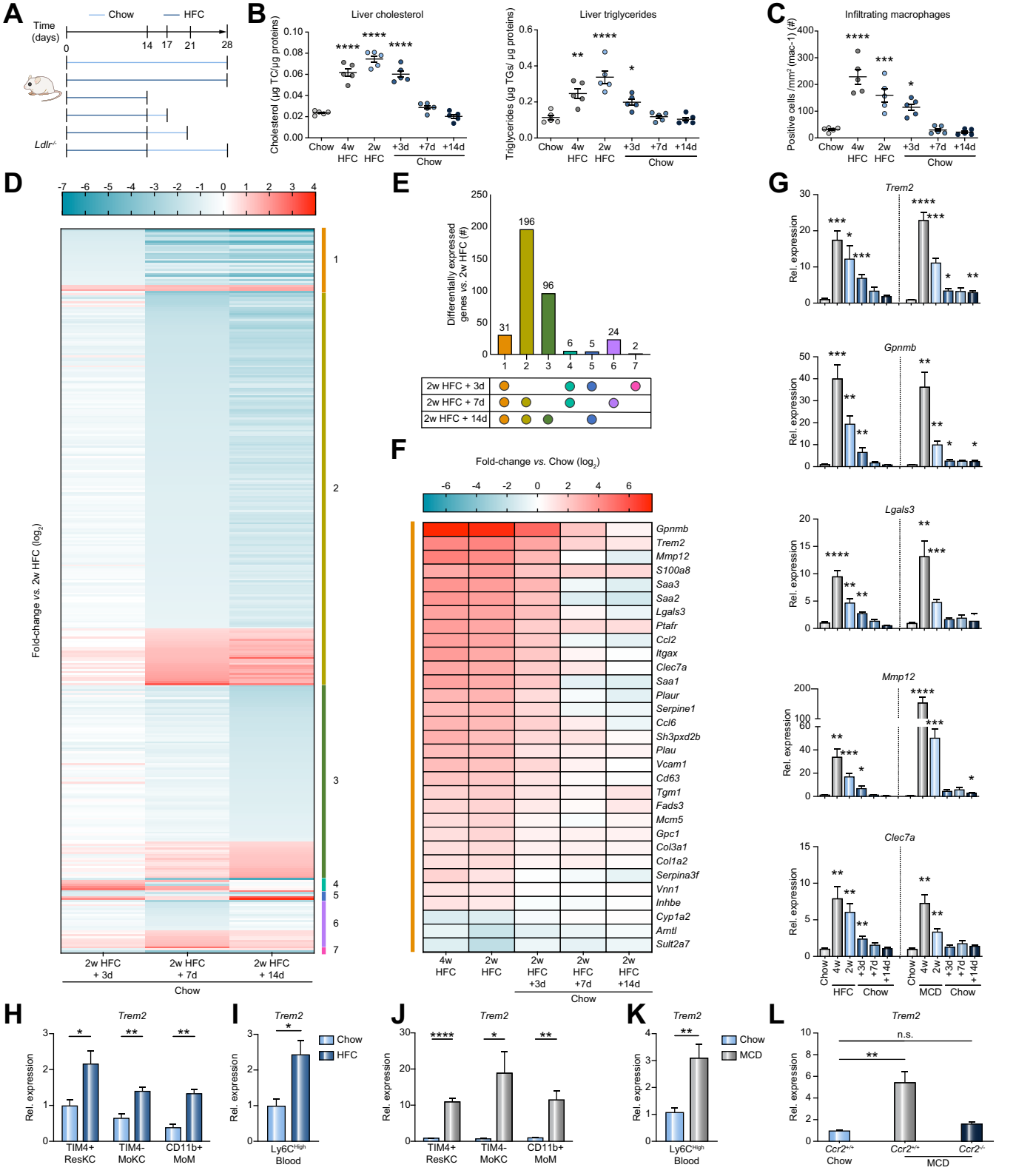

Fig. 1. Hepatic differential gene expression signature associated with diet-induced inflammation reflects dynamics of *Trem2*-expressing macrophages. (A) Experimental design of dietary intervention study in female *Ldlr*$^{-/-}$ mice. (B) Hepatic cholesterol and triglyceride levels normalized to liver protein content. (C) Hepatic infiltrating macrophages as assessed by immunohistochemical staining of liver sections for Mac-1. (D) Heatmap of genes differentially expressed compared to 2 weeks of HFC following 3, 7 and 14 days of dietary switching to chow, showing 7 distinct gene expression patterns. Data are derived from bulk RNA sequencing from whole liver tissue of mice following the dietary intervention pattern shown in Fig. 1A. Fold change represents expression (log_2) relative to expression in livers from 2-week HFC-fed mice. (E) Patterns of gene expression changes following dietary switching. Number of differentially expressed genes following the respective pattern are annotated above bars. (F) Heatmap of the 31 genes in cluster 1, whose expression is altered upon HFC and significantly

chemokines are produced, resulting in recruitment of leukocytes to areas of inflammation.[8] Moreover, ResKC are depleted during NASH followed by replenishment of their local niche by circulating bone marrow-derived monocytes that acquire KC features (MoKCs) and eventually take over their function.[9–13] Importantly, recent studies have demonstrated considerable heterogeneity among macrophages in the liver that may differentially influence disease progression via their interplay with other hepatic cells.[13–18] Yet, the specific functional properties of distinct macrophage populations, particularly the role of bone marrow-derived monocytes in the context of NASH are not fully understood and require better characterization.

Herein, using an unbiased approach to decipher factors and pathways contributing to hepatic inflammation during NAFLD, we found that murine steatohepatitis is associated with a hepatic transcriptomic profile characterized by hyperlipidemia-dependent induction of Triggering receptor expressed on myeloid cells 2 (*Trem2*). Previous single-cell RNA-sequencing analyses have shown that *Trem2*-expressing macrophages are present in the liver during obesity (lipid-associated macrophage, LAMs[19]), during murine NASH (NASH-associated macrophages or NAMs[20]) and in human and murine cirrhosis (scar-associated macrophages or SAMs[21]). Herein, we aimed to functionally characterize the role of bone marrow-derived TREM2$^+$ macrophage populations in NASH.

Materials and methods

A full description of the materials and methods used can be found in the supplementary methods.

Results

Hepatic gene expression profile in NAFLD reflects the dynamics of recruited TREM2-associated macrophages

In order to study factors involved in non-alcoholic hepatic inflammation, we designed a murine study using *Ldlr*$^{-/-}$ mice, which develop NAFLD with a human-like lipoprotein profile upon feeding a high-fat high-cholesterol (HFC) diet.[22,23] *Ldlr*$^{-/-}$ mice were placed on HFC diet for 2 or 4 weeks, while additional groups of mice were switched back to chow diet for 3, 7 or 14 days after 2 weeks of HFC diet (to study disease onset, while still allowing full disease reversal) or only received regular chow for 4 weeks (Fig. 1A). Upon HFC feeding, mice developed increased hepatic and plasma triglyceride and cholesterol levels that reverted to levels comparable to the chow group after 7 days of dietary switching, which was also reflected in histological changes (Fig. 1B and Fig. S1A,C). A similar pattern was observed in the accumulation of immune cells, including infiltrating macrophages (Mac1$^+$), neutrophils (Ly6G$^+$) and T cells (CD3$^+$) in the liver (Fig. 1C, S1B-C), and the hepatic gene expression levels of several proinflammatory cytokines (*Tnfa*, *Cxcl1*, *Cxcl2*; Fig. S1D). Moreover, in line with previous data illustrating that caloric restriction regulates peripheral monocyte numbers,[24] dietary switching reverted the increase in circulating inflammatory monocytes and neutrophils upon HFC diet feeding (Fig. S1E). These data indicate that early NAFLD progression is characterized by monocytosis and infiltrating immune cells that can be rapidly reverted by dietary intervention.

Transcriptomic profiling of whole liver tissue revealed 3 major transcriptomic patterns in the livers of HFC-fed mice compared to mice on chow (Fig. S2A). The majority of differential gene expression occurred early and persisted for the duration of the HFC diet (461 genes; 'sustained response'; Fig. S2A-B), while 264 genes were only altered after 4 weeks of HFC feeding ('late response') and 217 genes were only differently regulated in mice receiving 2 weeks HFC ('early response'). In line with our previous data,[23] hepatic inflammation during NAFLD is characterized by an innate immunity-associated gene expression signature likely arising from enhanced recruitment of various immune cells to the liver (Fig. S2C-D).

We next compared expression levels of the 'sustained response' genes in livers of mice switched to regular chow for 3, 7 and 14 days to mice on HFC diet for 2 weeks (Fig. 1D-E). The expression of 31 genes reverted to levels comparable to chow already by 3 days, suggesting these genes to be particularly responsive to diet-induced inflammation (Fig. 1E-F). A majority of these genes (*Gpnmb*, *Trem2*, *Mmp12*, *Lgals3*, *Itgax*, *Cd63*, *Clec7a)* have previously been found to be highly expressed in TREM2$^+$ macrophages also present in the livers of humans and mice with NASH,[19–21] suggesting that changes in hepatic gene expression in our murine model are determined by the presence of TREM2$^+$ macrophages in the liver.

Furthermore, we applied the methionine- and choline-deficient (MCD) diet model, which results in a more advanced NASH-like phenotype characterized by extensive inflammation and hepatic fibrosis[25,26] in a similar dietary intervention setting (Fig. S3A-E). Similar to the hypercholesterolemic HFC model, hepatic expression of TREM2$^+$ macrophage-related genes *Trem2*, *Gpnmb*, *Lgals3*, *Mmp12* and *Clec7a* was strongly increased upon MCD-induced NASH and reached expression levels comparable to the livers of chow-fed controls by 3-7 days after dietary switching (Fig. 1G). In addition, induction of hepatic *Trem2* expression was observed in the STAM model, which reflects multiple stages of progressive NASH[25–27] (Fig. S4A-B) and in mice receiving high-fat diet (HFD) (Fig. S4C-D), indicating that the induction of a TREM2-related gene signature represents a general feature of NAFLD.

reverted to levels comparable to livers of chow-fed mice by 3, 7 and 14 days after dietary switching. Fold change represents expression (log_2) relative to expression in livers of chow-fed mice. Genes are ranked based on the fold change after 2 weeks HFC diet *vs.* chow-fed mice. (G) Expression of indicated genes in livers of *Ldlr*$^{-/-}$ mice after the HFC dietary intervention shown in Fig. 1A and of wild-type mice following MCD dietary intervention shown in Fig. S3A. Data are shown relative to the respective chow-fed mice. (H) *Trem2* expression in sorted TIM4$^+$ ResKCs, TIM4$^-$ MoKCs and CD11b$^+$ MoMs of *Ldlr*$^{-/-}$ mice fed chow or HFC diet for 2 weeks. Data are shown relative to expression in ResKCs from chow-fed animals. (I) *Trem2* expression in sorted circulating Ly6C^{high} monocytes of *Ldlr*$^{-/-}$ mice fed chow or HFC diet for 2 weeks. (J) *Trem2* expression in sorted TIM4$^+$ ResKCs, TIM4$^-$ MoKCs and CD11b$^+$ MoMs of C57Bl6/J mice fed chow or MCD diet for 4 weeks. Data are shown relative to expression in ResKCs from chow-fed animals. (K) *Trem2* expression in sorted circulating Ly6C^{high} monocytes of C57Bl6/J mice fed chow or MCD diet for 4 weeks. (L) *Trem2 expression* in livers of chow or MCD-fed *Ccr2*$^{+/+}$ and *Ccr2*$^{-/-}$ mice. Data are shown relative to chow-fed *Ccr2*$^{+/+}$ mice. For B, C, G, H, I, J, K and L, data are shown as mean ± SEM of n = 4-9 mice per group. Significance is indicated compared to the respective chow group after applying one-way ANOVA with Bonferroni correction or 2-tailed unpaired Student's *t* test for comparing multiple or 2 groups respectively, after testing for normality. For D-F, n = 2 mice per group. $^*p \leq 0.05$, $^{**}p \leq 0.01$, $^{***}p \leq 0.001$, $^{****}p \leq 0.0001$. Abbreviations defined at the end of manuscript.

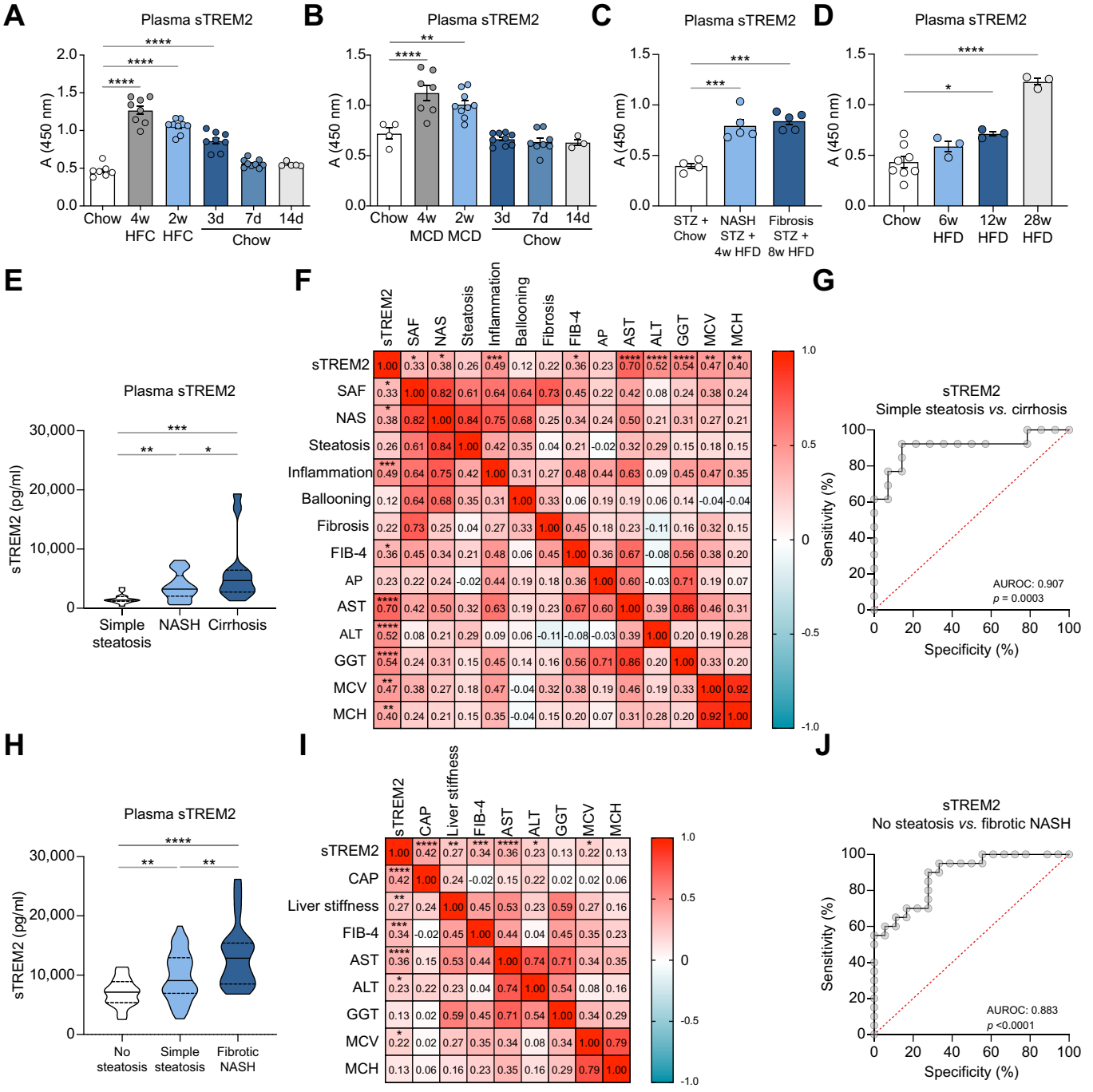

Fig. 2. Soluble TREM2 levels correlate with disease severity in mice and humans. (A) Plasma sTREM2 levels in chow-, HFC-fed and diet switched female *Ldlr*$^{-/-}$ mice during the dietary intervention study depicted in Fig. 1A. (B) Plasma sTREM2 levels in chow-, MCD-fed and diet switched male C57Bl6/J mice during the dietary intervention study depicted in Fig. S3A. (C) Plasma sTREM2 levels in STZ-injected male C57Bl6/J mice fed chow or a 46% HFD for 4 and 8 weeks. (D) Plasma sTREM2 levels in male C57Bl6/J mice fed chow or a 60% HFD for 6, 12 and 28 weeks. (E) Violin plot showing plasma sTREM2 levels in patients with biopsy-proven NAFLD; simple steatosis (n = 14), NASH (n = 30) and cirrhosis (n = 13). (F) Pearson correlation analysis of sTREM2 levels and histological scoring for SAF (Steatosis, Activity, Fibrosis), NAS, steatosis, inflammation, ballooning, fibrosis, FIB-4 scoring, and systemic liver disease markers ALP, AST, ALT, GGT, MCV and MCH. (G) AUROC analysis of sTREM2 levels in patients with biopsy-proven NAFLD, with simple steatosis (n = 14) or cirrhosis (n = 13). (H) Violin plot showing plasma sTREM2 levels in individuals classified into 'no steatosis' (n = 18), 'simple steatosis' (n = 59) or 'fibrotic NASH' (n = 20), based on CAP and liver stiffness (Fibroscan) measurements. (I) Pearson correlation analysis of sTREM2 levels and liver disease markers CAP, liver stiffness, FIB-4, AST, ALT, GGT, MCV and MCH. (J) AUROC analysis of sTREM2 levels in individuals classified as having 'no steatosis' (n = 18) or 'fibrotic NASH' (n = 20). For A-D, data shown as mean ± SEM and significance compared to respective chow-fed mice is indicated. For E and F, data shown as mean ± SEM. One-way ANOVA with Bonferroni correction was used for testing significance between multiple groups or unpaired 2-tailed Student's *t* test was used for comparing individual groups. **p* ≤0.05, ** *p* ≤0.01, *** *p* ≤0.001, **** *p* ≤0.0001. Abbreviations defined at the end of manuscript.

In order to pinpoint the cellular source of increased hepatic *Trem2* expression during NASH, we assessed *Trem2* mRNA levels in sorted TIM4^{+} ResKCs, TIM4^{-} MoKCs and CD11b^{+} monocyte-derived macrophages (MoMs) from livers (Fig. S3G-J),[12,13] as well as in circulating blood Ly6C^{high} monocytes. Compared to chow, *Trem2* expression was strongly induced in all 3 hepatic macrophage subsets in HFC- and particularly in MCD-fed mice (Fig. 1H, 1J, S3K-L). Remarkably, *Trem2* expression was also increased in circulating Ly6C^{high} monocytes in both dietary models (Fig. 1I, 1K, S3K-L), indicating increased *Trem2* expression on myeloid cells occurs both in the liver and in the periphery. Consistent with previous data,[11–15] we observed that the hepatic macrophage pool during NASH mainly consists of recruited MoMs, while ResKCs are depleted (Fig. S3G-J), indicating recruited MoMs are the main contributors to total hepatic *Trem2* levels. In line with this, mice deficient in CCR2, which have less recruited MoMs in the liver, failed to induce hepatic *Trem2* expression after MCD diet feeding (Fig. 1L, S3M-N). Moreover, the number of infiltrating macrophages (CD11b^{+}) positively correlated with the expression of *Trem2* in the liver in both dietary models (Fig. S1F, S3F). Therefore, our data demonstrate that the diet-sensitive hepatic gene expression profile reflects the dynamics of recruited *Trem2*-expressing monocytes.

Systemic soluble TREM2 levels are elevated during NASH in mice and humans

TREM2 occurs both in membrane-bound form and in soluble form, consisting of its ectodomain upon cleavage by A disintegrin and metalloproteinase (ADAM) 10 or ADAM17.[28] Given the strong induction of *Trem2* expression during murine NASH, we assessed the circulating levels of soluble TREM2 (sTREM2) in these mice. Intriguingly, plasma sTREM2 levels followed the same pattern as hepatic *Trem2* expression in *Ldlr*$^{-/-}$ mice on HFC diet and C57Bl6/J mice on MCD diet (Fig. 2A-B). Additionally, systemic sTREM2 levels were increased during steatohepatitis in the STAM model and in HFD-induced fatty liver disease (Fig. 2C-D). Consistent with the positive correlation between infiltrating macrophages and hepatic *Trem2* expression, plasma sTREM2 levels also significantly correlated with liver-infiltrating macrophages in HFC- and MCD-induced NASH (Fig. S5A-B), suggesting that sTREM2 is mostly MoM-derived.

Since TREM2^{+} macrophages were previously described in human cirrhotic livers,[21] we assessed whether systemic sTREM2 also associates with disease severity in a cohort of patients with biopsy-proven NAFLD. Intriguingly, patients diagnosed with cirrhosis showed significantly higher levels of sTREM2 than those with NASH or simple steatosis, while NASH patients also had elevated sTREM2 compared to people with steatosis only (Fig. 2E). Moreover, plasma sTREM2 correlated positively with multiple markers for liver disease, among them alanine aminotransferase (ALT), aspartate aminotransferase (AST), gamma-glutamyltransferase (GGT), histological NAFLD activity score and Fibrosis-4 (FIB-4)[29] scoring (Fig. 2F). To assess the accuracy of sTREM2 in distinguishing different stages of NAFLD, we performed an AUROC analysis. sTREM2 could distinguish patients with cirrhosis *vs.* simple steatosis (6,179 ± 1,538 pg/ml *vs.* 2,176 ± 328.7 pg/ml, AUROC 0.907, p = 0.0003; Fig. 2G) with very high accuracy.

In a second independent cohort consisting of patients who underwent ultrasonography-based Fibroscan measurements to determine liver disease status, patients classified as having fibrotic NASH also had significantly increased sTREM2 levels compared to patients without steatosis or with simple steatosis only (Fig. 2H). sTREM2 levels correlated significantly with specific liver disease parameters including the controlled attenuation parameter (a sonographic measure of steatosis), liver stiffness assessed by Fibroscan, ALT, AST and FIB-4 scoring (Fig. 2I). AUROC analysis revealed a clear distinction between 'fibrotic NASH' and patients without steatosis (13,298 ± 1,200 pg/ml *vs.* 7,069 ± 551.7 pg/ml, AUROC 0.883, p <0.0001; Fig. 2J) or with simple steatosis (9,730 ± 523.2 pg/ml, AUROC 0.695, p <0.0092, Fig. S5E). Plasma sTREM2 showed no correlations with metabolic parameters (*i.e.* BMI, LDL, HDL, total cholesterol, triglycerides) in the biopsy-proven cohort (Fig. S5C) and only mild correlations with plasma VLDL and triglycerides in the second cohort (Fig. S5D). Intriguingly, 2 established liver damage markers, ALT and AST, as well as FIB-4 fibrosis scoring, showed no or poorer predictive value in differentiating liver disease stages compared to sTREM2 (Fig. S5F-N). Overall, these data demonstrate the clinical relevance of macrophage-derived TREM2 and demonstrate that plasma sTREM2 can distinguish between absent or mild and advanced NASH with higher accuracy than traditional liver disease-associated parameters such as ALT and AST.

Trem2-expressing macrophages localize to areas of inflammation, oxidative stress and fibrosis

In order to gain insight into the interaction of TREM2^{+} macrophage subsets with the local niche and to assess their tissue localization, we performed spatial transcriptomics on 6 liver sections from *Ldlr*$^{-/-}$ mice fed chow (n = 3) or HFC diet for 2 weeks (n = 3) from 2 independent studies using 2 10X Visium Spatial gene expression slides. Uniform manifold approximation and projection (UMAP) clustering and principal component analysis revealed a clear separation of gene expression profiles in spots of livers from HFC-fed mice compared to chow-fed controls. We also observed a second separation based on experiment, suggesting that external study factors (*e.g.* time of experiment, cage effects, fasting time) may have affected hepatic gene expression (Fig. S6A-B). Importantly, in line with our bulk RNA-sequencing results, the expression of *Trem2, Gpnmb* and *Lgals3* was significantly upregulated (to a similar extent) in the livers and spots containing immune cells (*Ptprc*$^{+}$) of all 3 HFC-fed mice compared to controls, irrespective of potential batch effects (Fig. 3A-C, S6C). While no spots were positive for the combination of *Trem2*, *Gpnmb* and *Lgals3* in livers of chow-fed mice, up to 10% of tissue-covered spots were triple-positive in livers of HFC-fed mice (*Trem2*$^{+}$*Gpnmb*$^{+}$*Lgals3*$^{+}$, Fig. S6D). Consistent with our findings in sorted hepatic macrophage subsets, we identified *Trem2*$^{+}$*Gpnmb*$^{+}$*Lgals3*$^{+}$ spots positive for either ResKC (*Adgre1*$^{+}$*Clec4f*$^{+}$*Timd4*$^{+}$), MoKC (*Adgre1*$^{+}$*Clec4f*$^{+}$*Timd4*$^{-}$) or MoM

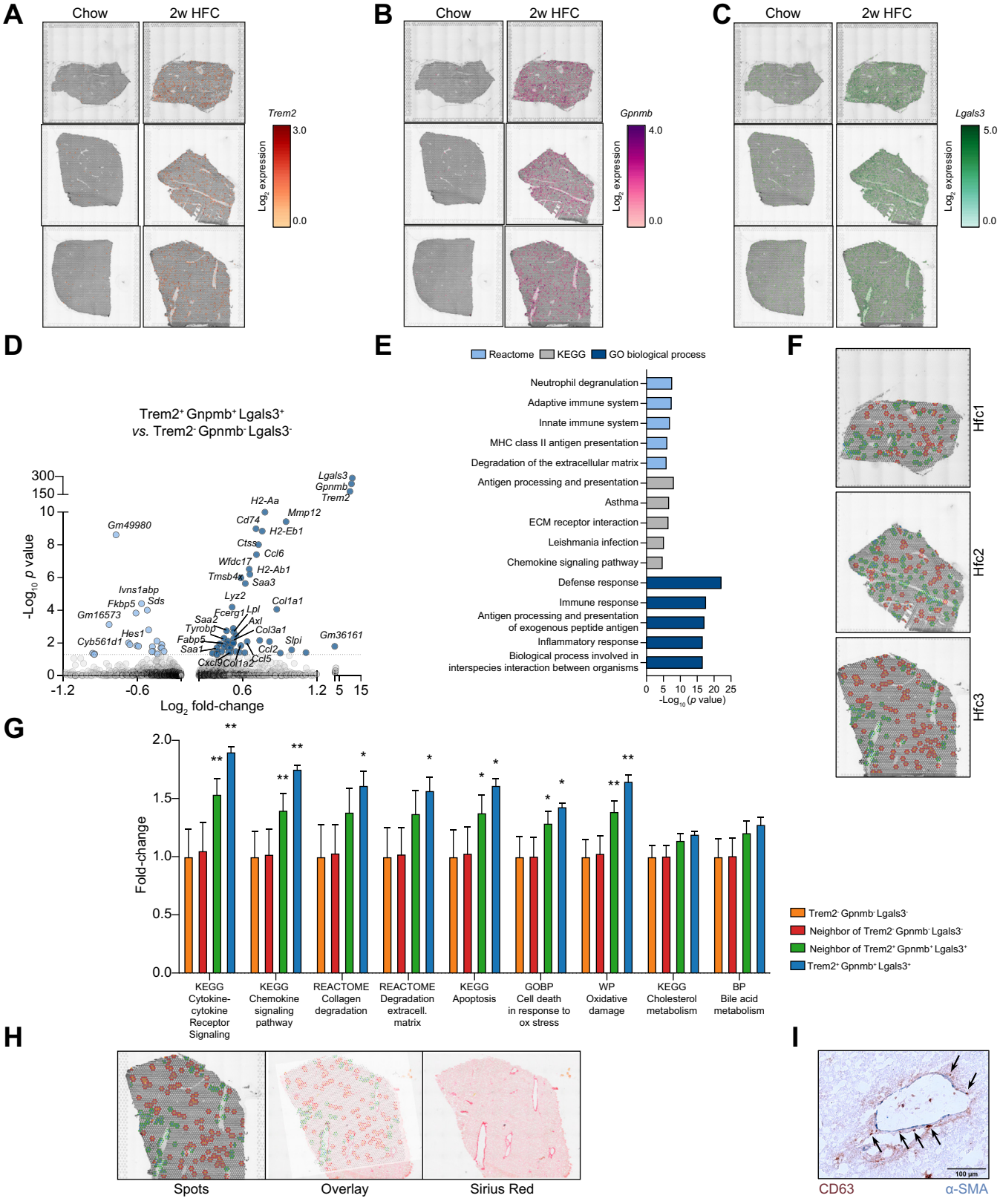

Fig. 3. *Trem2*-expressing macrophages localize to areas of inflammation and fibrosis in steatotic livers. (A-C) Spatial expression of *Trem2* (A, red), *Gpnmb* (B, purple), *Lgals3* (C, green) in liver sections of chow- and 2 week HFC-fed female *Ldlr*$^{-/-}$ mice. Color scales indicate $\log_2$ expression of the respective genes relative to expression in all other spots. (D) Volcano plot showing significantly up- and downregulated genes in TREM2$^+$ (*Trem2*$^+$*Gpnmb*$^+$*Lgals3*$^+$) spots compared to TREM2$^-$ (*Trem2*$^-$*Gpnmb*$^-$*Lgals3*$^-$) spots in liver sections of HFC-fed *Ldlr*$^{-/-}$ mice. Negative $\log_2$ fold change indicates downregulation, positive $\log_2$ fold change indicates upregulation in TREM2$^+$ spots. Non-significantly differentially expressed genes (p >0.05) or with a $\log_2$ fold change between -0.25 and 0.25 are shown in grey. (E)

(*Ly6c2*$^+$) markers (Fig. S6E-F). Moreover, the expression of *Trem2* and TREM2$^+$ macrophage-related markers (*Gpnmb, Lgals3, Cd9, Cd63, Tyrobp, Mmp12*) was higher in spots containing ResKC, MoKC and MoM than in spots containing other immune cells (*Ptprc*$^+$*Adgre1*$^-$*Clec4f*$^+$*Timd4*$^-$*Ly6c2*$^-$) or non-immune cells (*Ptprc*$^-$*Adgre1*$^-$*Clec4f*$^+$*Timd4*$^-$*Ly6c2*$^-$) to a similar extent in all 3 HFC livers (Fig. S6G-H).

To evaluate the transcriptomic profile at spots occupied by TREM2$^+$ macrophages, we selected *Trem2*$^+$*Gpnmb*$^+$*Lgals3*$^+$ (TREM2$^+$) spots and compared them to *Trem2*$^-$*Gpnmb*$^-$*Lgals3*$^-$ (TREM2$^-$) spots within HFC livers. Gene ontology analysis revealed that TREM2$^+$ spots were enriched for genes associated with inflammatory processes (*Ccl2, Ccl5, Ccl6*), lipid metabolism (*Lpl, Ctss*), liver injury (*Saa1, Saa2, Saa3*), as well as fibrosis and extracellular matrix remodeling (*Col1a1, Col1a2, Col3a1, Mmp12*) (Fig. 3D-E). To further investigate the local microenvironment of *Trem2*-expressing cells, we manually selected all the immediate neighboring spots of TREM2$^+$ leukocytes (*Trem2*$^+$*Gpnmb*$^+$*Lgals3*$^+$*Ptprc*$^+$) and TREM2$^-$ leukocytes (*Trem2*$^-$*Gpnmb*$^-$*Lgals3*$^-$*Ptprc*$^+$) in the livers of HFC-fed mice (Fig. 3F). Interestingly, besides more expression of TREM2-related markers (Fig. S6I), spots containing TREM2$^+$ leukocytes and their direct neighborhoods showed significant enrichment of gene sets related to inflammation, collagen degradation and cell death compared to TREM2$^-$ cells and their neighboring spots, while expression of genes related to cholesterol and bile acid metabolism were not different (Fig. 3G, S6J). In addition, TREM2$^+$ spots and neighborhoods were predominantly detected at sites of collagen deposition as indicated by Sirius Red staining, while cells staining positive for CD63, a surrogate marker for TREM2$^+$ macrophages, localized to alpha-smooth muscle actin-rich areas (Fig. 3H-I). Taken together, these findings imply the prominent involvement of *Trem2*-expressing macrophages in regions of inflammation, cell death, fibrosis and extracellular matrix remodeling.

Hematopoietic TREM2 deficiency exacerbates steatohepatitis

Our data suggested an important contribution of recruited leukocytes to the hepatic accumulation of macrophages in the context of NASH. Indeed, mice fed an MCD diet display a relative depletion of ResKCs and an increase of MoKCs and MoMs (Fig. S3I, S7A-B). Moreover, using CD45.1+ bone marrow-chimeric mice, we could show that all 3 hepatic macrophage populations are predominantly derived from recruited hematopoietic cells in bone marrow-transplanted mice fed an MCD diet, albeit with a generally low contribution of ResKCs in this model (Fig. S7B-C). To address the role of hematopoietic TREM2 in NASH, wild-type mice were lethally irradiated to receive bone marrow from *Trem2*$^{-/-}$ or *Trem2*$^{+/+}$ littermates and put on an MCD diet for 4 weeks (Fig. 4A). Compared to wild-type-transplanted mice, sTREM2 levels were greatly reduced in mice transplanted with TREM2-deficient bone marrow, in line with the hematopoietic origin of systemic sTREM2 (Fig. 4B). Mice with hematopoietic TREM2 deficiency developed significantly increased liver injury and steatohepatitis, as indicated by increased plasma ALT levels (Fig. 4C) and hepatic triglyceride and lipid content (Fig. 4D-E). The heightened inflammation was mirrored in increased infiltrating macrophages (CD11b$^+$) (Fig. 4F-G) and the expression of proinflammatory genes *Saa1* and *Il1b*, which have been implicated in NASH[30–32] (Fig. 4H). Moreover, there was significantly more cell death, as evidenced by increased numbers of TUNEL-positive cells (Fig. 4I), higher percentage of AnnexinV$^+$ F4/80$^+$ KCs and a similar trend for AnnexinV$^+$ CD11b$^+$ MoMs (Fig. 4J). This was mirrored in increased cell death in *Trem2*$^{-/-}$ *vs.* *Trem2*$^{+/+}$ bone marrow-derived macrophages (BMDMs) cultured *in vitro* without and with IL-4, a known inducer of *Trem2*[33] (Fig. 4K). Importantly, *Trem2*$^{-/-}$-bone marrow-chimeric mice developed markedly aggravated fibrosis, as indicated by immunohistochemical detection of Sirius Red and Masson's Trichrome staining (Fig. 4L-M). Moreover, expression of profibrotic genes *Acta2, Col1a1* and *Col3a1* and levels of hydroxyproline and COL1A1 were increased in livers of *Trem2*$^{-/-}$ bone marrow-chimeric mice (Fig. 4N-P). Consistent with this, we also found that hypercholesterolemic *Ldlr*$^{-/-}$ mice with hematopoietic (Fig. S8A-F) or global (Fig. S8G-J) TREM2 deficiency developed aggravated steatohepatitis upon HFC diet. Overall, these findings indicate a protective function for bone marrow-derived TREM2 in the development of NASH and liver fibrosis.

Hematopoietic TREM2 modulates the composition of the hepatic myeloid cell compartment during NASH

To gain insights into the effects of hematopoietic TREM2 deficiency on the hepatic immune cell composition during NASH, we performed single-cell RNA-sequencing of pooled CD45+ cells sorted from livers of 4-week-old MCD-fed mice transplanted with TREM2-deficient or wild-type bone marrow (Fig. S9). Following quality control and doublet exclusion, unsupervised Louvain clustering and UMAP projection of 10,589 cells (5,607 *Trem2*$^{+/+}$, 4,982 *Trem2*$^{-/-}$) resulted in 24 clusters representing different cell subsets that were annotated based on differentially expressed hematopoietic lineage-defining genes, revealing changes in the immune cell landscape (*e.g.* T cells) upon hematopoietic TREM2 deficiency (Fig. S9A-D).

Since *Trem2* was primarily expressed in hepatic macrophages as well as circulating Ly6C^{high} monocytes during NASH, we performed sub-clustering of macrophages, KCs and monocytes (clusters 2, 3, 5, 10, 18, 22) to further dissect changes in the heterogeneous hepatic myeloid compartment in the context of hematopoietic TREM2 deficiency. Sub-clustering revealed 13 clusters that were identified based on the expression of lineage-defining markers (Fig. 5A-B, S10A-E). Of these, cluster 0 showed

Reactome, KEGG and GO Biological Process analysis of differentially expressed genes in TREM2$^+$ *vs.* TREM2$^-$ spots in HFC-fed livers. Top 5 significantly altered pathways are presented. (F) Images showing selection of TREM2$^-$ spots (*Trem2*$^-$*Gpnmb*$^-$*Lgals3*$^-$*Ptprc*$^+$, orange) and their direct neighboring spots (red), and TREM2$^+$ areas (*Trem2*$^+$*Gpnmb*$^+$*Lgals3*$^+$*Ptprc*$^+$, blue) and their direct neighboring spots (green) in the liver sections of 2-week HFC-fed *Ldlr*$^{-/-}$ mice. (G) Spatial transcriptomic assessment of enrichment of indicated gene set modules in TREM2$^+$ and TREM2$^-$ spots and their direct neighbors as defined in Fig. 3F. Data are shown as fold change of the average enrichment within indicated spots compared to TREM2$^-$ spots. One-way ANOVA was used for testing significance between multiple groups. $^*p \leq 0.05$, $^{**}p \leq 0.01$. (H) Overlay (middle) of spatial slide Hfc3 indicating spots defined as TREM2$^+$, TREM2$^-$ and their neighbors (left), with the adjacent serial cryosection stained for fibrosis using Sirius Red (right). (I) Colocalization of CD63$^+$ cells and α-SMA (40x magnification) in liver after 4 weeks MCD diet. Abbreviations defined at the end of manuscript.

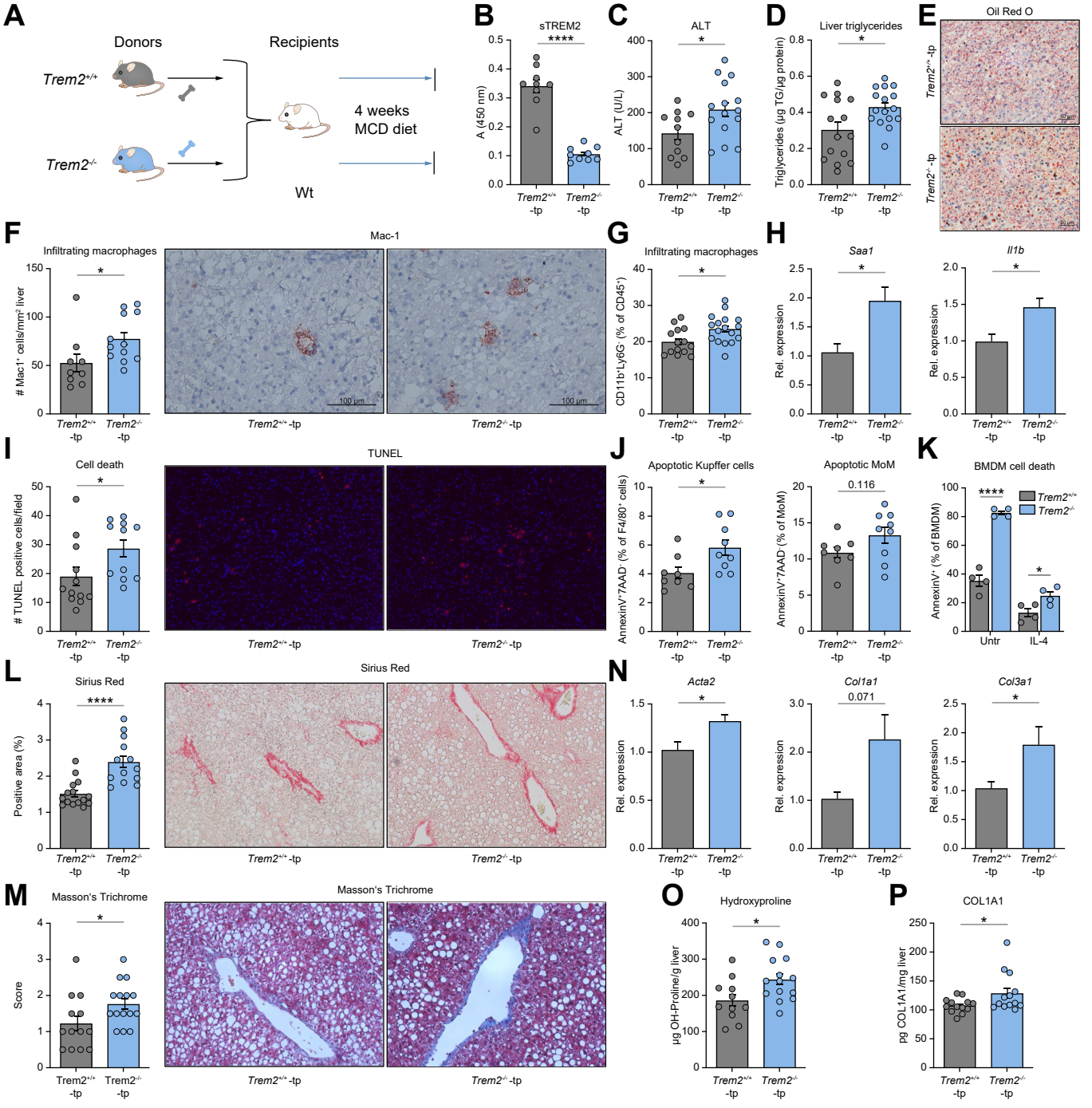

Fig. 4. Hematopoietic TREM2 deficiency exacerbates MCD-induced NASH. (A) Experimental design. C57Bl6/J male recipients were lethally irradiated and received bone marrow from *Trem2*$^{+/+}$ (*Trem2*$^{+/+}$-tp, grey) and *Trem2*$^{-/-}$ (*Trem2*$^{-/-}$-tp, blue) littermates. After 6-week recovery, mice were placed on MCD diet for 4 weeks. (B) Plasma sTREM2 levels. (C) Plasma ALT levels. (D) Hepatic triglyceride levels. (E) Representative pictures of Oil Red O staining of liver sections (20x magnification). (F) Quantification and representative images of infiltrating macrophages as assessed by Mac-1^{+} staining of liver sections. (G) Infiltrating macrophages (CD45^{+}Ly6G^{-}CD11b^{+}F4/80$^{-/low}$) as assessed by flow cytometry. (H) Relative expression of *Saa1* and *Il1b* in whole liver tissue assessed by qPCR. Data are shown relative to *Trem2*$^{+/+}$-tp mice. (I) Quantification of TUNEL+ cells per field and representative images of liver sections stained with DAPI and TUNEL (20x magnification). (J) Evaluation of apoptotic Kupffer cells (CD45^{+}F4/80^{+}CD11b$^{+/-}$) and apoptotic MoMs (CD45^{+}Ly6G^{-}CD11b^{+}F4/80$^{-/low}$) using Annexin V staining as assessed by flow cytometry. (K) Evaluation of apoptotic BMDMs isolated from *Trem2*$^{+/+}$ and *Trem2*$^{-/-}$ littermates cultured *in vitro*. (L) Quantification and representative images of Sirius Red^{+} area of liver sections (20x magnification). (M) Scoring of Masson's Trichrome staining and representative images of liver sections. (N) Hepatic expression of *Acta2*, *Col1a1* and *Col3a1*. Data are shown relative to *Trem2*$^{+/+}$-tp mice. (O) Hepatic hydroxyproline content. (P) Hepatic collagen I alpha 1 content. Data shown as mean ± SEM of n = 11-15 mice per group. Significance is indicated between *Trem2*$^{-/-}$-tp and *Trem2*$^{+/+}$-tp mice or *Trem2*$^{-/-}$ and *Trem2*$^{+/+}$ BMDMs (K) after applying 2-tailed unpaired Student's *t* test comparing 2 groups after testing for normality. **p* ≤0.05, *****p* ≤0.0001. Abbreviations defined at the end of manuscript.

high expression of *Spp1, Cd9, Gpnmb, Lgals3, Cd63, Cd36, Lpl, Fabp5,* several cathepsins and *Mmp12,* resembling previously described pre-moKCs and MMP12^{+} macrophages.[13] Some of these signatures were also seen in cluster 2, which were also enriched for similar markers, but were negative for *Spp1.* Cluster 7 resembled hepatic LAMs[13] and were further characterized by elevated expression of *Cx3cr1*, *Ccr2* and *Itgam*, suggesting they represent a monocyte-derived population (Figs 5C-E and S10B-D).

Since clusters 0, 2 and 7 showed the strongest enrichment in *Trem2* (Fig. 5C) and its associated markers *Gpnmb*, *Cd9*, *Itgax*, *Lgals3* and partially *Spp1* (Fig. S10B-D), we focused on these cell clusters. Notably, *Trem2* enrichment associated with expression of *Ccr2* and *Cxc3cr1* (Fig. 5D-E), further supporting monocyte-derived *Trem2* expression in the context of NASH.

Importantly, TREM2 deficiency resulted in downregulation of several SAM/LAM-related genes in these clusters including *Gpnmb*, *Cd63*, *Cd36*, *Lpl, Fabp4* and *Fabp5*, while the percentage of cells expressing these genes within these clusters was similar between *Trem2*-deficient and wild-type bone marrow recipients (Fig. 5F-H, S10F). Moreover, comparison of the cluster composition between the conditions suggests potential reductions in the relative proportion of LAM-like clusters 0 and 2 and increases in monocyte clusters 4 and 10 (Fig. 5B, S10G). Thus, TREM2 may be partially required for the adoption of a SAM/LAM-like phenotype or the differentiation, maintenance or survival of these cells.

Expression changes in LAM/SAM-related genes were also reflected in gene expression levels in the total liver of MCD-fed *Trem2*$^{-/-}$ bone marrow-chimeric mice (Fig. 5I) and in *in vitro*-cultured BMDMs from *Trem2*$^{-/-}$ or *Trem2*$^{+/+}$ littermates (Fig. 5J). This suggests impaired ability to handle lipids efficiently, in line with the exacerbated steatosis we observed in *Trem2*-deficient mice during NASH (Fig. 4D-E) as well as impaired *in vitro* foam cell formation in peritoneal macrophages from *Trem2*$^{-/-}$ mice upon culture with oxidized LDL (Fig. 5K). Furthermore, TREM2 deficiency was associated with increased expression of various proinflammatory cytokines and chemokines (Fig. 5F-H), among them *Ccl2, Ccl5*, *Cxcl9*, *Cxcl10*, as well as the inflammasome-associated genes *Il1b, Nlrp3* and *Il1a,* which were previously shown to be associated with fibrosis.[30–32] Additionally, there was a downregulation of *Anxa1* and *Prdx1*, which were previously implicated in hepatic fibrosis via their anti-inflammatory effects and regulation of oxidative stress, respectively.[34,35] Similar changes in the expression of inflammatory genes were found in the livers of *Trem2*$^{-/-}$ bone marrow-chimeric mice and BMDMs from *Trem2*$^{-/-}$ mice (Fig. 5L-M).

Moreover, multiple clusters showed downregulation in *Mmp12* encoding matrix metalloproteinase 12, which plays a key role in the degradation of extracellular matrix and the resolution of liver fibrosis.[36,37] Given the observed profibrotic phenotype upon hematopoietic TREM2 deficiency (Fig. 4L-P) and the association of TREM2 with SAMs, we assessed the clusters of *Trem2*$^{+/+}$ and *Trem2*$^{-/-}$ mice for enrichment of the SAM signature (as described in[21]). In line with the increased expression of *Trem2* and its associated genes in these clusters, the SAM signature was particularly enriched in clusters 0, 2 and 7 in *Trem2*$^{+/+}$, but not in *Trem2*$^{-/-}$ mice (Fig. 5N), suggesting a loss of the fibrosis-associated SAM phenotype. Consistent with this, we found decreased expression of *Mmp12* as well as increased expression of the profibrotic genes *Tgfb1* and *Timp1* in the livers of *Trem2*$^{-/-}$ mice (Fig. 5O) and untreated and IL-4-stimulated *Trem2*$^{-/-}$ BMDMs (Fig. 5P). To functionally address the fibrogenic potential of these cells, murine 3T3 fibroblasts were incubated with conditioned media collected from *Trem2*$^{-/-}$ or *Trem2*$^{+/+}$ BMDMs. Conditioned medium from IL-4-treated *Trem2*$^{-/-}$ BMDMs increased the expression of fibroblast marker genes *Acta2, Col1a1* and *Col3a1* compared to medium from IL-4-treated wild-type BMDMs, suggesting increased profibrogenic potential in TREM2-deficient BMDMs (Fig. 5Q), in line with the increased fibrosis observed in our *in vivo* studies and the reduced MMP12 content in the livers of MCD-fed *Trem2*$^{-/-}$-bone marrow-chimeric mice (Fig. 5R). Thus, hematopoietic TREM2 deficiency alters the hepatic myeloid compartment, resulting in impaired lipid handling, increased inflammation and fibrosis due to the loss of SAM-like macrophages.

Discussion

The origin of TREM2^{+} macrophages in the liver has been a subject of debate. While NAMs were originally proposed to represent a ResKC population,[20] SAMs were described as monocyte-derived cells.[21] Herein, we describe that in addition to ResKCs, recruited MoMs and MoKCs in the liver, *Trem2* is already induced in circulating Ly6C^{high} monocytes during NASH. Although stimulation of certain nuclear receptors, such as liver X receptor and retinoid X receptor, has been proposed to promote expression of *Trem2* in myeloid cells,[38,39] the exact trigger and mechanism by which hepatic macrophage subsets and circulating monocytes upregulate TREM2 remains to be identified.

While our data in the present study are inconclusive regarding the role of TREM2 on self-renewing ResKCs, our findings that *Trem2*-expressing recruited macrophages prevent aggravated steatohepatitis and fibrosis might have important clinical implications, as interventions to block infiltration of immune cells, such as cenicriviroc, a dual CCR2/CCR5 chemokine receptor antagonist have been tested,[40] albeit with limited success.[41–43] Furthermore, recent data showed that abrogation of recruited MoMs upon *Ccr2*-deficiency exacerbated liver disease development in mice, possibly due to diminished recruitment of anti-fibrotic TREM2^{+} cells.[14] Therefore, our data argue for more precise immune cell targeting and differentiation between pathological and protective circulating immune cell populations in developing therapeutic interventions.

Previously it has been shown that during NASH, monocyte-derived cells replenish the KC niche.[9–15] While we show that hepatic TREM2 expression is primarily dependent on CCR2-mediated monocyte recruitment, the functional role of TREM2 on ResKCs remains uncertain. As irradiation and bone marrow transplantation itself causes aberrant replacement of ResKCs with monocyte-derived cells, the isolated contribution of TREM2 on ResKCs cannot be fully elucidated in our model and should be dissected in future studies.

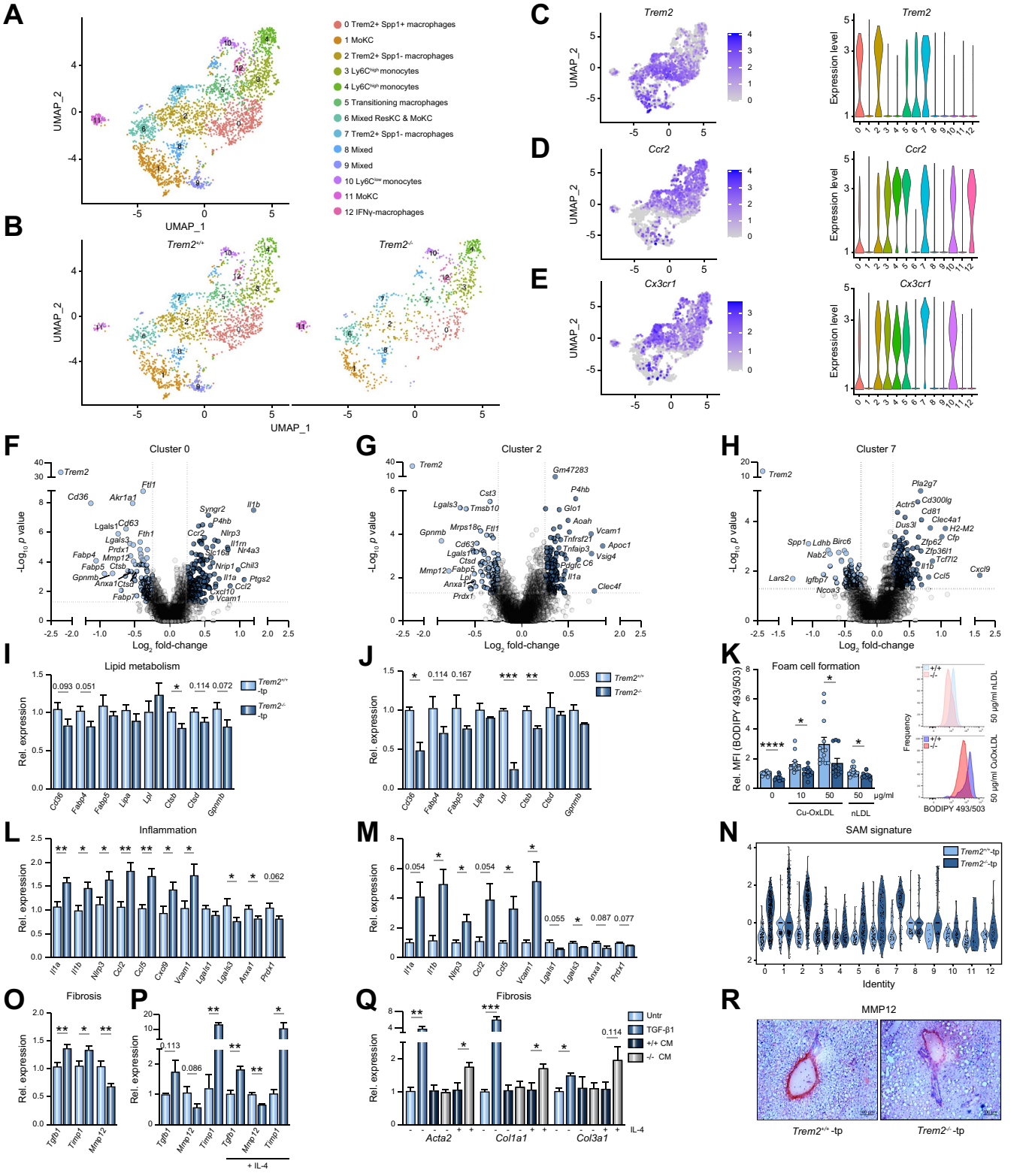

Fig. 5. Hematopoietic TREM2 deficiency alters the hepatic myeloid compartment during MCD-induced NASH. (A) UMAP resulting from reclustering of macrophage- and monocyte-containing clusters. Clusters were annotated based on expression of lineage-defining genes shown in Fig. S10. (B) UMAP split by condition, *Trem2*$^{+/+}$- (left) and *Trem2*$^{-/-}$-bone marrow chimeric mice (right). (C-E) Feature and violin plots indicating the expression of *Trem2* (C), *Ccr2* (D) and *Cx3cr1* (E) projected onto the UMAP and across different clusters, respectively. (F-H) Volcano plots showing differentially expressed genes between *Trem2*$^{+/+}$- and *Trem2*$^{-/-}$-bone marrow chimeric mice in cluster 0 (F) cluster 2 (G) and cluster 7 (H). Negative $\log_2$ fold change indicates downregulation (light blue), positive $\log_2$ fold change indicates upregulation in *Trem2*$^{-/-}$- (dark blue) relative to *Trem2*$^{+/+}$-transplanted mice. Non-significantly differentially expressed genes (p >0.05) or genes with a $\log_2$ fold change between -0.25 and 0.25 are shown in grey. (I) Expression of indicated genes in livers of MCD-fed C57Bl6/J mice from study shown in Fig. 4. (J) Expression of indicated genes in BMDMs isolated from *Trem2*$^{+/+}$ and *Trem2*$^{-/-}$ littermates cultured *in vitro*. (K) *In vitro* foam cell formation in

Our study also identified plasma sTREM2 levels as a sensitive marker for fibrotic NASH in patients with NAFLD. Whether higher sTREM2 levels are the result of more cleavage by ADAM10/17 proteases or represent systemic markers of increased hepatic TREM2$^+$ macrophage turnover or cell death remains to be shown. Additionally, while recent data in animal models of Alzheimer's disease suggest that both soluble and sustained membrane-bound TREM2 can exert protective functions,[44–46] the functional properties of sTREM2 in NASH remain to be clarified. Still, our data from 2 independent cohorts suggest that inclusion of systemic sTREM2 levels can improve the accuracy and predictive power of available panels of non-invasive tests for liver injury and fibrosis in NASH.

Consistent with earlier findings showing that differentiation of microglia to disease-associated macrophages,[47] adipose tissue macrophages to LAMs[19] or the emergence of restorative macrophages during resolution following chemically induced liver injury[48] are partially dependent on the presence of TREM2, we observed that hematopoietic TREM2 deficiency may impair the ability of recruited monocytes to fully adopt a SAM/LAM phenotype in the liver during NASH, as suggested by the changes in the expression of SAM/LAM-related genes. Although the mechanism by which TREM2 deficiency interferes with the accumulation of LAMs/SAMs is not entirely clear, regulation of cell survival, particularly under conditions of stress including tissue damage and inflammation has been shown.[49,50] In line with this, we observed more cell death in macrophages in the absence of TREM2 both in hepatic macrophages in the context of NASH and in *in vitro*-cultured BMDMs. On the other hand, we cannot exclude a more direct role for TREM2 in cellular differentiation, as has been proposed for disease-associated macrophages,[47] LAMs[19] and osteoclasts.[51,52] More insight into the role of TREM2 as a determinant of macrophage plasticity is required.

Mechanistically, our data imply that multiple aspects contribute to exacerbated liver disease in the context of hematopoietic TREM2 deficiency. We observed a phenotypic switch in the hepatic myeloid compartment in mice lacking hematopoietic TREM2, favoring expression of proinflammatory chemokines and cytokines. Among these, the prominent T-cell chemoattractants *Ccl5*, *Cxcl9* and *Cxcl10* have been implicated in human and murine NASH.[30,53–55] In line with this, our single-cell sequencing indicated an increased proportion of T cells within the hepatic immune cell landscape, suggesting enhanced T-cell infiltration upon TREM2 deficiency, thereby potentially promoting NASH.[56] Notably, recent work suggests that TREM2 may also play a direct role in the suppression of T-cell activation.[57,58]

TREM2 has been implicated as a lipid-sensing receptor.[49,59] Our data demonstrate dysregulated expression of several genes involved in lipid metabolism as well as functional impairment of lipid handling in the absence of TREM2. Indeed, we observed significantly increased steatosis in our models of advanced, MCD-induced NASH and HFC-induced NAFLD, in line with a recent study that found increased steatosis during mild, early HFD-induced steatosis in mice with global TREM2 deficiency.[60]

Our spatial transcriptomics analysis and histological staining indicate that TREM2$^+$ macrophages localize to areas of increased fibrosis, in line with previous data that found TREM2$^+$ SAMs to localize to fibrotic areas in human cirrhotic livers.[21] However, in contrast to the proposed profibrotic function of SAMs,[21] our single-cell sequencing data suggest that exacerbated liver fibrosis observed upon TREM2 deficiency is linked to a loss of SAM gene expression profile in multiple myeloid cell clusters, and potentially a reduced proportion of SAM-like cells. Notably, our data reveals reduced expression of *Mmp12* and increased expression of its negative regulator *Timp1*, which actively participate in extracellular matrix degradation and the resolution of fibrosis.[37] On the other hand, *Trem2*-deficient macrophages may have an enhanced fibrogenic potential due to the secretion of soluble mediators such as TGF-β1 or the release of soluble factors during increased cell death, which is supported by our observation using conditioned media from *Trem2*$^{-/-}$ BMDMs in fibroblast activation assays *in vitro*.

Taken together, our data not only demonstrate the origin and function of TREM2$^+$ macrophages in NASH, but also define sTREM2 in plasma as a circulating marker that tracks disease progression. Functionally, we show that bone marrow-derived *Trem2* expression is key for the generation of anti-fibrotic macrophages that inhibit the proinflammatory transcriptional program of myeloid cells in the liver to limit NASH, thereby rendering TREM2 a particularly interesting putative therapeutic target to promote tissue remodeling and reverse NASH progression.

Abbreviations

ADAM, A disintegrin and metalloproteinase; ALP, alkaline phosphatase; ALT, alanine aminotransferase; AST, aspartate aminotransferase; BMDMs, bone marrow-derived macrophages; CCR2, C-C chemokine receptor type 2; GGT, gamma-glutamyltransferase; HFC, High-fat high-cholesterol; HFD, high-fat diet; LAM, lipid-associated macrophage; MAFLD, metabolic dysfunction-associated fatty liver disease; MCD, methionine and choline-deficient; MCH, mean corpuscular hemoglobin; MCV, mean corpuscular volume; MoKCs, monocyte-derived Kupffer cells; MoMs, monocyte-derived macrophages; NAFLD, non-

thioglycollate-elicited macrophages isolated from *Trem2*$^{+/+}$ and *Trem2*$^{-/-}$ littermates assessed by BODIPY493/503 staining, shown relative to untreated *Trem2*$^{+/+}$ macrophages (data from 4 independent experiments, total n = 11-13/group; unpaired 2-tailed Student's *t* test). (L) Expression of indicated genes in livers of MCD-fed C57Bl6/J mice from study shown in Fig. 4. (M) Expression of indicated genes in BMDMs isolated from *Trem2*$^{+/+}$ and *Trem2*$^{-/-}$ littermates cultured *in vitro*. (N) Violin plot showing the gene module enrichment scores of the SAM signature[21] per cluster, separated for *Trem2*$^{+/+}$- (light blue) and *Trem2*$^{-/-}$-bone marrow chimeric mice (dark blue). (O) Expression of indicated genes in livers of MCD-fed C57Bl6/J mice from study shown in Fig. 4. (P) Expression of indicated genes in BMDMs isolated from *Trem2*$^{+/+}$ and *Trem2*$^{-/-}$ littermates cultured *in vitro*. (Q) Expression of fibroblast activation genes in 3T3 fibroblasts cultured with TGF-β1 (positive control) or in conditioned media from BMDMs from *Trem2*$^{+/+}$ and *Trem2*$^{-/-}$ littermates (n = 4/group) cultured with or without IL-4. Data are shown relative to each *Trem2*$^{+/+}$ condition, compared by unpaired Student's *t* test. (R) Representative images showing MMP12 staining of liver sections of MCD-fed *Trem2*$^{+/+}$- (left) and *Trem2*$^{-/-}$-bone marrow chimeric mice (right) from study shown in Fig. 4. For I, L, O, data are shown as mean ± SEM, relative to expression in livers of *Trem2*$^{+/+}$-transplanted mice. For J, M, and P, data are shown as mean ± SEM, relative to expression in BMDMs obtained from *Trem2*$^{+/+}$ mice. Significance is indicated after applying 2-tailed unpaired Student's *t* test comparing 2 groups after testing for normality. $^*p \leq 0.05$, $^{**}p \leq 0.01$, $^{***}p \leq 0.001$, $^{****}p \leq 0.0001$. Abbreviations defined at the end of manuscript.

alcoholic fatty liver disease; NAMs, NASH-associated macrophages; NAS, NAFLD activity score; NASH, non-alcoholic steatohepatitis; ResKCs, resident Kupffer cells; SAM, scar-associated macrophage; sTREM2, soluble TREM2; STZ, streptozotocin; TREM2, triggering receptor expressed on myeloid cells 2.

Financial support
TH is funded by a Veni grant (NWO; 91619012), 'Right-On-Time' grant (MLDS; W019-28) and Zukunftskollegs grant (FWF; ZK81B). FP was supported by the Doctoral program Cell Communication in Health and Disease (CCHD; FWF_W1205-B09) funded by the Austrian Science Fund. SK received funding from the Austrian Science Fund (SFB F54 and F61). MT received funding from the Austrian Science Fund (SFB F7310). CJB was supported by grants of the Austrian Science Fund (SFB F54) and the Leducq Foundation (TNE-20CVD03).

Conflict of interest
The authors declare no conflict of interest.

Please refer to the accompanying ICMJE disclosure forms for further details.

Authors' contributions
TH, FP designed and performed the studies, acquired and analyzed the data, wrote and edited the manuscript. MGK designed and performed studies, acquired and analyzed the data and critically revised the manuscript. DR, CH, LG, LES provided technical assistance and acquired part of the data. NPM performed animal studies and critically revised the manuscript. AH performed animal studies. SK provided the mouse strain and critically revised the manuscript. SD, MB acquired and analyzed the spatial transcriptomics data and critically revised the manuscript. LH, MK, RP, MT provided human samples/data and critically revised the manuscript. MF, HH, DW acquired and analyzed the single-cell RNA-sequencing data and critically revised the manuscript. CJB designed the studies, analyzed the data, wrote and edited the manuscript.

Data availability statement
The data generated in this study are available via the NCBI GEO database (accession number GSE207138) and from corresponding authors, TH or CJB, upon reasonable request.

Acknowledgements
We thank the people from the Core Facility Flow Cytometry, Genomics and Imaging of the Medical University of Vienna for their support and critical help in the acquisition of our data. We thank Latifa Bakiri for her help with the *in vitro* fibrosis assay, Claudia Fuchs for the hydroxyproline measurements, Christoph Bock for his advice on the spatial transcriptomics analyses and Helmuth Haslacher for his help assessing the human sTREM2 measurements. We also express our gratitude to all animal caretakers from the Medical University of Vienna responsible for animals used in this project.

Supplementary data
Supplementary data to this article can be found online at https://doi.org/10.1016/j.jhep.2022.06.004.

References
Author names in bold designate shared co-first authorship

[1] **Eslam M**, **Newsome PN**, Sarin SK, Anstee QM, Targher G, Romero-Gomez M, et al. A new definition for metabolic dysfunction-associated fatty liver disease: an international expert consensus statement. J Hepatol 2020;73:202–209.
[2] Younossi Z, Anstee QM, Marietti M, Hardy T, Henry L, Eslam M, et al. Global burden of NAFLD and NASH: trends, predictions, risk factors and prevention. Nat Rev Gastroenterol Hepatol 2018;15:11–20.
[3] Charlton MR, Burns JM, Pedersen RA, Watt KD, Heimbach JK, Dierkhising RA. Frequency and outcomes of liver transplantation for nonalcoholic steatohepatitis in the United States. Gastroenterology 2011;141:1249–1253.
[4] Younossi ZM, Blissett D, Blissett R, Henry L, Stepanova M, Younossi Y, et al. The economic and clinical burden of nonalcoholic fatty liver disease in the United States and Europe. Hepatology 2016;64:1577–1586.
[5] Buzzetti E, Pinzani M, Tsochatzis EA. The multiple-hit pathogenesis of non-alcoholic fatty liver disease (NAFLD). Metabolism 2016;65:1038–1048.
[6] Wang H, Mehal W, Nagy LE, Rotman Y. Immunological mechanisms and therapeutic targets of fatty liver diseases. Cell Mol Immunol 2021;18:73–91.
[7] Kazankov K, Jorgensen SMD, Thomsen KL, Moller HJ, Vilstrup H, George J, et al. The role of macrophages in nonalcoholic fatty liver disease and nonalcoholic steatohepatitis. Nat Rev Gastroenterol Hepatol 2019;16:145–159.
[8] Krenkel O, Tacke F. Liver macrophages in tissue homeostasis and disease. Nat Rev Immunol 2017;17:306–321.
[9] Beattie L, Sawtell A, Mann J, Frame TCM, Teal B, de Labastida Rivera F, et al. Bone marrow-derived and resident liver macrophages display unique transcriptomic signatures but similar biological functions. J Hepatol 2016;65:758–768.
[10] van de Laar L, Saelens W, De Prijck S, Martens L, Scott CL, Van Isterdael G, et al. Yolk sac macrophages, fetal liver, and adult monocytes can colonize an empty niche and develop into functional tissue-resident macrophages. Immunity 2016;44:755–768.
[11] Scott CL, Zheng F, De Baetselier P, Martens L, Saeys Y, De Prijck S, et al. Bone marrow-derived monocytes give rise to self-renewing and fully differentiated Kupffer cells. Nat Commun 2016;7:10321.
[12] **Tran S**, **Baba I**, Poupel L, Dussaud S, Moreau M, Gelineau A, et al. Impaired Kupffer cell self-renewal alters the liver response to lipid overload during non-alcoholic steatohepatitis. Immunity 2020;53:627–640 e625.
[13] Remmerie A, Martens L, Thone T, Castoldi A, Seurinck R, Pavie B, et al. Osteopontin expression identifies a subset of recruited macrophages distinct from Kupffer cells in the fatty liver. Immunity 2020;53:641–657 e614.
[14] Daemen S, Gainullina A, Kalugotla G, He L, Chan MM, Beals JW, et al. Dynamic shifts in the composition of resident and recruited macrophages influence tissue remodeling in NASH. Cell Rep 2021;34:108626.
[15] **Seidman JS**, **Troutman TD**, Sakai M, Gola A, Spann NJ, Bennett H, et al. Niche-specific reprogramming of epigenetic landscapes drives myeloid cell diversity in nonalcoholic steatohepatitis. Immunity 2020;52:1057–1074 e1057.
[16] **Guilliams M**, **Bonnardel J**, **Haest B**, Vanderborght B, Wagner C, Remmerie A, et al. Spatial proteogenomics reveals distinct and evolutionarily conserved hepatic macrophage niches. Cell 2022;185:379–396.e338.
[17] **Bonnardel J**, **T'Jonck W**, Gaublomme D, Browaeys R, Scott CL, Martens L, et al. Stellate cells, hepatocytes, and endothelial cells imprint the Kupffer cell identity on monocytes colonizing the liver macrophage niche. Immunity 2019;51:638–654 e639.
[18] **Wen Y**, **Lambrecht J**, Ju C, Tacke F. Hepatic macrophages in liver homeostasis and diseases-diversity, plasticity and therapeutic opportunities. Cell Mol Immunol 2021;18:45–56.
[19] **Jaitin DA**, **Adlung L**, **Thaiss CA**, **Weiner A**, **Li B**, Descamps H, et al. Lipid-associated macrophages control metabolic homeostasis in a trem2-dependent manner. Cell 2019;178:686–698 e614.
[20] **Xiong X**, **Kuang H**, **Ansari S**, **Liu T**, Gong J, Wang S, et al. Landscape of intercellular crosstalk in healthy and NASH liver revealed by single-cell secretome gene analysis. Mol Cell 2019;75:644–660 e645.
[21] Ramachandran P, Dobie R, Wilson-Kanamori JR, Dora EF, Henderson BEP, Luu NT, et al. Resolving the fibrotic niche of human liver cirrhosis at single-cell level. Nature 2019;575:512–518.

[22] Bieghs V, Van Gorp PJ, Wouters K, Hendrikx T, Gijbels MJ, van Bilsen M, et al. LDL receptor knock-out mice are a physiological model particularly vulnerable to study the onset of inflammation in non-alcoholic fatty liver disease. PLoS One 2012;7:e30668.
[23] **Busch CJ**, **Hendrikx T**, Weismann D, Jackel S, Walenbergh SM, Rendeiro AF, et al. Malondialdehyde epitopes are sterile mediators of hepatic inflammation in hypercholesterolemic mice. Hepatology 2017;65:1181–1195.
[24] Jordan S, Tung N, Casanova-Acebes M, Chang C, Cantoni C, Zhang D, et al. Dietary intake regulates the circulating inflammatory monocyte pool. Cell 2019;178:1102–1114 e1117.
[25] Oligschlaeger Y, Shiri-Sverdlov R. NAFLD preclinical models: more than a handful, less of a concern? Biomedicines 2020;8:28.
[26] Nevzorova YA, Boyer-Diaz Z, Cubero FJ, Gracia-Sancho J. Animal models for liver disease - a practical approach for translational research. J Hepatol 2020;73:423–440.
[27] Febbraio MA, Reibe S, Shalapour S, Ooi GJ, Watt MJ, Karin M. Preclinical models for studying NASH-driven HCC: how useful are they? Cell Metab 2019;29:18–26.
[28] Feuerbach D, Schindler P, Barske C, Joller S, Beng-Louka E, Worringer KA, et al. ADAM17 is the main sheddase for the generation of human triggering receptor expressed in myeloid cells (hTREM2) ectodomain and cleaves TREM2 after Histidine 157. Neurosci Lett 2017;660:109–114.
[29] Sterling RK, Lissen E, Clumeck N, Sola R, Correa MC, Montaner J, et al. Development of a simple noninvasive index to predict significant fibrosis in patients with HIV/HCV coinfection. Hepatology 2006;43:1317–1325.
[30] Berres ML, Koenen RR, Rueland A, Zaldivar MM, Heinrichs D, Sahin H, et al. Antagonism of the chemokine Ccl5 ameliorates experimental liver fibrosis in mice. J Clin Invest 2010;120:4129–4140.
[31] Kamari Y, Shaish A, Vax E, Shemesh S, Kandel-Kfir M, Arbel Y, et al. Lack of interleukin-1alpha or interleukin-1beta inhibits transformation of steatosis to steatohepatitis and liver fibrosis in hypercholesterolemic mice. J Hepatol 2011;55:1086–1094.
[32] **Mridha AR**, **Wree A**, Robertson AAB, Yeh MM, Johnson CD, Van Rooyen DM, et al. NLRP3 inflammasome blockade reduces liver inflammation and fibrosis in experimental NASH in mice. J Hepatol 2017;66:1037–1046.
[33] Turnbull IR, Gilfillan S, Cella M, Aoshi T, Miller M, Piccio L, et al. Cutting edge: TREM-2 attenuates macrophage activation. J Immunol 2006;177:3520–3524.
[34] Locatelli I, Sutti S, Jindal A, Vacchiano M, Bozzola C, Reutelingsperger C, et al. Endogenous annexin A1 is a novel protective determinant in nonalcoholic steatohepatitis in mice. Hepatology 2014;60:531–544.
[35] **Zhang Z**, **Ji Z**, He J, Lu Y, Tian W, Zheng C, et al. Guanine nucleotide-binding protein G(i) subunit alpha 2 exacerbates NASH progression by regulating peroxiredoxin 1-related inflammation and lipophagy. Hepatology 2021;74:3110–3126.
[36] Kisseleva T, Brenner D. Molecular and cellular mechanisms of liver fibrosis and its regression. Nat Rev Gastroenterol Hepatol 2021;18:151–166.
[37] Ramachandran P, Pellicoro A, Vernon MA, Boulter L, Aucott RL, Ali A, et al. Differential Ly-6C expression identifies the recruited macrophage phenotype, which orchestrates the regression of murine liver fibrosis. Proc Natl Acad Sci U S A 2012;109:E3186–E3195.
[38] **Daniel B**, **Nagy G**, Hah N, Horvath A, Czimmerer Z, Poliska S, et al. The active enhancer network operated by liganded RXR supports angiogenic activity in macrophages. Genes Dev 2014;28:1562–1577.
[39] Savage JC, Jay T, Goduni E, Quigley C, Mariani MM, Malm T, et al. Nuclear receptors license phagocytosis by trem2+ myeloid cells in mouse models of Alzheimer's disease. J Neurosci 2015;35:6532–6543.
[40] Lefere S, Devisscher L, Tacke F. Targeting CCR2/5 in the treatment of nonalcoholic steatohepatitis (NASH) and fibrosis: opportunities and challenges. Expert Opin Investig Drugs 2020;29:89–92.
[41] Friedman SL, Ratziu V, Harrison SA, Abdelmalek MF, Aithal GP, Caballeria J, et al. A randomized, placebo-controlled trial of cenicriviroc for treatment of nonalcoholic steatohepatitis with fibrosis. Hepatology 2018;67:1754–1767.
[42] **Ratziu V**, **Sanyal A**, Harrison SA, Wong VW, Francque S, Goodman Z, et al. Cenicriviroc treatment for adults with nonalcoholic steatohepatitis and fibrosis: final analysis of the phase 2b CENTAUR study. Hepatology 2020;72:892–905.
[43] Vuppalanchi R, Noureddin M, Alkhouri N, Sanyal AJ. Therapeutic pipeline in nonalcoholic steatohepatitis. Nat Rev Gastroenterol Hepatol 2021;18:373–392.
[44] **Schlepckow K**, **Monroe KM**, **Kleinberger G**, Cantuti-Castelvetri L, Parhizkar S, Xia D, et al. Enhancing protective microglial activities with a dual function TREM2 antibody to the stalk region. EMBO Mol Med 2020;12:e11227.
[45] Zhong L, Chen XF, Wang T, Wang Z, Liao C, Wang Z, et al. Soluble TREM2 induces inflammatory responses and enhances microglial survival. J Exp Med 2017;214:597–607.
[46] Zhong L, Xu Y, Zhuo R, Wang T, Wang K, Huang R, et al. Soluble TREM2 ameliorates pathological phenotypes by modulating microglial functions in an Alzheimer's disease model. Nat Commun 2019;10:1365.
[47] **Keren-Shaul H**, **Spinrad A**, **Weiner A**, **Matcovitch-Natan O**, Dvir-Szternfeld R, Ulland TK, et al. A unique microglia type associated with restricting development of Alzheimer's disease. Cell 2017;169:1276–1290 e1217.
[48] Coelho I, Duarte N, Barros A, Macedo MP, Penha-Gonçalves C. Trem-2 promotes emergence of restorative macrophages and endothelial cells during recovery from hepatic tissue damage. Front Immunol 2020;11:616044.
[49] Wang Y, Cella M, Mallinson K, Ulrich JD, Young KL, Robinette ML, et al. TREM2 lipid sensing sustains the microglial response in an Alzheimer's disease model. Cell 2015;160:1061–1071.
[50] Wu K, Byers DE, Jin X, Agapov E, Alexander-Brett J, Patel AC, et al. TREM-2 promotes macrophage survival and lung disease after respiratory viral infection. J Exp Med 2015;212:681–697.
[51] Cella M, Buonsanti C, Strader C, Kondo T, Salmaggi A, Colonna M. Impaired differentiation of osteoclasts in TREM-2-deficient individuals. J Exp Med 2003;198:645–651.
[52] **Otero K**, **Shinohara M**, **Zhao H**, Cella M, Gilfillan S, Colucci A, et al. TREM2 and β-catenin regulate bone homeostasis by controlling the rate of osteoclastogenesis. J Immunol 2012;188:2612–2621.
[53] Seki E, De Minicis S, Gwak GY, Kluwe J, Inokuchi S, Bursill CA, et al. CCR1 and CCR5 promote hepatic fibrosis in mice. J Clin Invest 2009;119:1858–1870.
[54] Tacke F, Zimmermann HW, Berres ML, Trautwein C, Wasmuth HE. Serum chemokine receptor CXCR3 ligands are associated with progression, organ dysfunction and complications of chronic liver diseases. Liver Int 2011;31:840–849.
[55] Zhang X, Shen J, Man K, Chu ES, Yau TO, Sung JC, et al. CXCL10 plays a key role as an inflammatory mediator and a non-invasive biomarker of non-alcoholic steatohepatitis. J Hepatol 2014;61:1365–1375.
[56] Sutti S, Albano E. Adaptive immunity: an emerging player in the progression of NAFLD. Nat Rev Gastroenterol Hepatol 2020;17:81–92.
[57] **Katzenelenbogen Y**, **Sheban F**, **Yalin A**, Yofe I, Svetlichnyy D, Jaitin DA, et al. Coupled scRNA-seq and intracellular protein activity reveal an immunosuppressive role of TREM2 in cancer. Cell 2020;182:872–885.e819.
[58] Molgora M, Esaulova E, Vermi W, Hou J, Chen Y, Luo J, et al. TREM2 modulation remodels the tumor myeloid landscape enhancing anti-PD-1 immunotherapy. Cell 2020;182:886–900.e817.
[59] Yeh FL, Wang Y, Tom I, Gonzalez LC, Sheng M. TREM2 binds to apolipoproteins, including APOE and CLU/APOJ, and thereby facilitates uptake of amyloid-beta by microglia. Neuron 2016;91:328–340.
[60] **Hou J**, **Zhang J**, Cui P, Zhou Y, Liu C, Wu X, et al. TREM2 sustains macrophage-hepatocyte metabolic coordination in nonalcoholic fatty liver disease and sepsis. J Clin Invest 2021:131.